Valuation of Vulnerable European Options in Garch Diffusion Models*†

Tinghe Zhang‡, Xingchun Wang

Abstract

In this paper, we study vulnerable European options in Garch Diffusion models. We consider the stochastic volatilities of both underlying assets and counterpart assets and extend the Garch Diffusion model to a bi-dimensional case for a more thorough analysis of options with default risk. And we introduce a broader pricing model incorporating a time-varying correlation coefficient with the market assets. Based on the proposed model, we obtain an approximate solution for the vulnerable European option price via means of characteristic function transform. Numerical results are presented to illustrate the impacts of stochastic volatility components and systematic risk on vulnerable option prices.

Keywords: Vulnerable Options; Garch Diffusion Models; Stochastic Correlation Coefficient; Counterparty Default Risk.

JEL classification: G13

1 Introduction

This paper investigates the pricing of vulnerable options under the continuous-time Garch Diffusion model. Since the financial crisis of 2007-2008, default risk has had a major influence on the price of

*Tinghe Zhang is at the School of Insurance and Economics, University of International Business and Economics, Beijing 100029, China. Xingchun Wang is at the School of International Trade and Economics, University of International Business and Economics, Beijing 100029, China.

†This is a working manuscript. Not yet submitted for publication. Please do not cite without permission.

‡Corresponding author. Email:tingherhea@163.com

financial derivatives, especially on these traded in the over-the-counter (OTC) markets. As noted by Arora et al. (2012) and Brigo et al. (2014), the lack of centralized exchanges that guarantee payment fulfillment highlights the need for default risk to be included into valuation frameworks.

Actually, the pricing issue of derivatives with default risk has been investigated in the literature. For instance, For instance, Arora et al. (2012) demonstrate how counterparty default risk is priced in the Credit Default Swap (CDS) markets. Leung and Kwok (2005) perform the valuation of CDS with unilateral counterparty risk. Brigo et al. (2014) extend their analysis to the valuation of CDS with bilateral default risk under collateralization. Crepey (2012a, 2012b) focuses on the valuation and hedging of OTC derivatives with bilateral default risk under funding constraints. We refer to Brigo et al. (2014) for pricing cases across different asset classes. In addition to credit default swaps, options with default risk have also been studied. Assuming that options are the only liability of the counterparty, Johnson and Stulz (1987) are the first to model default risk in a structural framework, creating an option pricing model for vulnerable options. Klein (1996) extends the work of Johnson and Stulz (1987) by considering other liabilities held by the option writer, thus providing a more comprehensive approach to pricing vulnerable options. Ma et al. (2020) have integrated the impact of stochastic interest rates and leverage effects into the SV framework, providing a more comprehensive understanding of the factors influencing option prices.

GARCH diffusion models are initially proposed by Nelson (1990) and stand out as an effective tool for capturing the temporal dynamics of financial time series data. Nelson (1990) proved that when the sampling frequency increases, the GARCH(1,1) model converges weakly to the GARCH diffusion model according to the distribution. Although we can not get the closed solution of the European option price under the non-affine GARCH diffusion model, Christofersen et al. (2019) shows that the GARCH diffusion model can better describe the price movement of financial assets than many other continuous time SV models (including Heston model), and more accurate option prices can be obtained based on the GARCH diffusion model. This model possesses several desirable properties; it is positive, mean-reverting, and characterized by a stable inverse Gamma distribution, satisfying the restriction that both historical and implied variances are positive (Scott, 1987; Xu, 1994; Jorion, 1995; Guo, 1996). It also aligns with the observed behavior of variance appearing to be stable and mean-reverting. Moreover, the GARCH diffusion model allows for rich patterns of behavior in volatility and asset prices, generating high autocorrelations in the squares of the

log-returns at a given order, large kurtosis, and finite unconditional moments, which have been empirically observed (Genon-Catalot et.al, 2000).

In this paper, we work under GARCH diffusion models to price vulnerable options. More specifically, we start by describing the dynamics of the market index in order to establish a connection between the counterparty's assets and the underlying asset. As in the Capital Asset Pricing Model (CAPM), betas are incorporated to represent the asset's sensitivity to systematic risk. In addition, the stochastic correlation (coefficient) between the counterparty's assets and the underlying asset is captured. In some sense, the proposed GARCH diffusion models extend the one in Nelson (1990) to a bi-dimensional case.

By deriving an approximate expression of the joint characteristic function, we successfully obtain an approximate pricing formula of vulnerable options in the proposed GARCH diffusion models. Finally, we check the accuracy of the approximate pricing formula by comparing with the Monte Carlo simulation methods. In numerical section, numerical experiments are conducted to illustrate the results. Parameter values for the market portfolio are borrowed from Bakshi et al. (1997), and those for the idiosyncratic volatility of the underlying asset are taken from Wang (2017), as listed in Table 1. The base case assumes a total volatility for the underlying asset of 0.23, equivalent to the average volatility of BB-rated firms as indicated in Zhang et al. (2009). Then, option values under constant volatilities and stochatic volatilities are reported for comparison.

Compared with previous studies, there are at least three contributions in this paper. The first one is that we propose a more general pricing model, in which the volatilities of the counterparty's assets and the underlying asset are stochastic, while Ma et al. (2020) employ a geometric Brownian motion to describe the dynamics of the counterparty's assets. Second, in the proposed Garch Diffusion models, the stochastic correlation (coefficient) between the counterparty's assets and the underlying asset changes stochastically over time, making the model in this paper be quite different from Ma et al. (2020). In Ma et al. (2020), the correlation coefficient between the counterparty's assets and the underlying asset is constant. Third, to our best knowledge, this paper is the first to extend GARCH models in Nelson (1990) to a bi-dimensional case. Moreover, it could be easily extended to the multi-dimensional case for valuing multi-asset options.

The rest of the paper is organized as follows. In Section 2, Garch Diffusion models are introduced and the approximate closed-form pricing formula of vulnerable options is derived using

the approximate joint characteristic function. Section 3 performs numerical analysis and Section 4 concludes this paper. The detailed proofs are shown in the Appendix.

2 Vulnerable European Options in Garch Diffusion Models

In this section, we consider vulnerable European options in Garch Diffusion models. In order to establish a connection between the dynamics of the counterparty's assets and the underlying asset, here we start by describing the dynamics of the market index, which obviously represents a common risk factor. More specifically, our formulation not only captures the time-varying correlation (coefficient) between the return of the counterparty's assets and the underlying asset's return, but also preserves the appealing aspects of Garch Diffusion models.

2.1 Garch Diffusion Models

Assume that a probability space $(\Omega, \mathcal{F}, \mathbb{Q})$ equipped with the filtration $\{\mathscr{F}_t\}_{t\geq 0}$, describes the uncertainty of the economy, where $\mathbb{Q}$ is a risk-neutral probability measure. Suppose that the market index's risk-neutral dynamics are driven by

$$\begin{cases} \frac{\mathrm{d}M_t}{M_t} = r\mathrm{d}t + \sqrt{Z_t^{(0)}}\mathrm{d}B_t, \\ \mathrm{d}Z_t^{(0)} = \kappa_0(\theta_0 - Z_t^{(0)})\mathrm{d}t + \sigma_0 Z_t^{(0)}\mathrm{d}L_t, \end{cases} \tag{2.1}$$

where B_t and L_t are two standard Brownian motions with a correlation coefficient ρ_0. It is obvious that the discounted value of the market index $e^{-rt}M_t$ is a martingale under $\mathbb{Q}$. Additionally, κ_0, θ_0 and σ_0 are constants.

Next, we suppose that the dynamics of the underlying asset are driven by the following process,

$$\begin{cases} \frac{\mathrm{d}S_t}{S_t} - r\mathrm{d}t = \beta_1(\frac{\mathrm{d}M_t}{M_t} - r\mathrm{d}t) + \sqrt{Z_t^{(1)}}\mathrm{d}B_t^{(1)}, \\ \mathrm{d}Z_t^{(1)} = \kappa_1(\theta_1 - Z_t^{(1)})\mathrm{d}t + \sigma_1 Z_t^{(1)}\mathrm{d}L_t^{(1)}, \end{cases} \tag{2.2}$$

where $B_t^{(1)}$ and $L_t^{(1)}$ are two standard Brownian motions with a correlation coefficient ρ_1, and κ_1, θ_1 and σ_1 are constants. In the above dynamics, the values of the underlying asset are affected by both systematic risk $\beta_1(\frac{\mathrm{d}M_t}{M_t} - r\mathrm{d}t)$ and idiosyncratic risk $\sqrt{Z_t^{(1)}}\mathrm{d}B_t^{(1)}$, where β_1 captures the underlying asset's sensitivity to the market index, and has a consistent form with the one in the capital asset pricing model (CAPM) as shown in Subsection 2.2. In a word, the risk sources of systematic risk and idiosyncratic risk are captured by $(B_t^{(0)}, L_t^{(0)})$ and $(B_t^{(1)}, L_t^{(1)})$, respectively.

In what follows, we follow Klein (1996) and Wang (2020) to employ typical structural approaches to investigate counterparty default risk. Similar to the above form of the underlying asset, we suppose that the values of the counterparty's assets are driven by the following process,

$$\begin{cases} \frac{\mathrm{d}V_t}{V_t} - r\mathrm{d}t = \beta_2(\frac{\mathrm{d}M_t}{M_t} - r\mathrm{d}t) + \sqrt{Z_t^{(2)}}\mathrm{d}B_t^{(2)}, \\ \mathrm{d}Z_t^{(2)} = \kappa_2(\theta_2 - Z_t^{(2)})\mathrm{d}t + \sigma_2 Z_t^{(2)}\mathrm{d}L_t^{(2)}, \end{cases} \tag{2.3}$$

where $B_t^{(2)}$ and $L_t^{(2)}$ are two standard Brownian motions with a correlation coefficient ρ_2, and κ_2, θ_2 and σ_2 are constants. Obviously, $(B_t^{(2)}, L_t^{(2)})$ captures idiosyncratic risk of the counterparty's assets, and therefore we further assume that $(B_t^{(0)}, L_t^{(0)})$, $(B_t^{(1)}, L_t^{(1)})$ and $(B_t^{(2)}, L_t^{(2)})$ are independent of each other.[1]

The above proposed Garch Diffusion models extend the one in Nelson (1990) to a bi-dimensional case in some sense, and could be easily extended to the multi-dimensional case in order to investigate multi-asset options such as basket options (with default risk). In addition, the stochastic correlation (coefficient) between the return of the counterparty's assets and the underlying asset's return is captured in the above proposed Garch Diffusion models as shown in the following subsection.

2.2 Stochastic Correlation (Coefficient)

In this subsection, we first show that the beta values have a consistent form with the one in the capital asset pricing model (CAPM), and then focus on the stochastic correlation (coefficient) between the return of the counterparty's assets and the underlying asset's return.

In the proposed Garch Diffusion models, the returns of the underlying asset are influenced by two distinct types of disturbances: idiosyncratic shocks and market shocks, and the beta describes how shocks on the market index impact the return of the underlying asset. Indeed, we have the

[1] This means that stochastic processes are independent of those in different parentheses.

following form of β_1,

$$\begin{aligned}\frac{\mathrm{Cov}_t\left(\frac{dS}{S},\frac{dM}{M}\right)}{\mathrm{Var}_t\left(\frac{dM}{M}\right)} &= \frac{\mathrm{Cov}_t\left(\beta_1\sqrt{Z_t^{(0)}}dB_t+\sqrt{Z_t^{(1)}}\mathrm{d}B_t^{(1)},\sqrt{Z_t^{(0)}}dB_t\right)}{\mathrm{Var}_t\left(rdt+\sqrt{Z_t^{(0)}}dB_t\right)}\\ &= \frac{\mathrm{Cov}_t\left(\beta_1\sqrt{Z_t^{(0)}}dB_t,\sqrt{Z_t^{(0)}}dB_t\right)}{\mathrm{Var}_t\left(\sqrt{Z_t^{(0)}}dB_t\right)}\\ &= \beta_1.\end{aligned}$$

It can be seen that β_1 indeed reflects the underlying asset's sensitivity to market or systematic risk, and has a consistent form with the one in the capital asset pricing model (CAPM). Through the same deduction, we can obtain that β_2 also captures the sensitivity of the counterpart's assets to systemic risk,

$$\beta_2 = \frac{\mathrm{Cov}_t\left(\frac{dV}{V},\frac{dM}{M}\right)}{\mathrm{Var}_t\left(\frac{dM}{M}\right)}.$$

In what follows, we focus our attention on the stochastic correlation (coefficient) between the return of the counterparty's assets and the underlying asset's return. From the dynamics of the underlying asset and the counterparty's assets, we deduce that the covariance between the return of the counterparty's assets and the underlying asset's return is formulated as follows,

$$\begin{aligned}\mathrm{Cov}_t\left(\frac{dS}{S},\frac{dV}{V}\right) &= \mathrm{Cov}_t\left(\beta_1\left(\frac{dM_t}{M_t}-rdt\right)+\sqrt{Z_t^{(1)}}dB_t^{(1)},\beta_2\left(\frac{dM_t}{M_t}-rdt\right)+\sqrt{Z_t^{(2)}}dB_t^{(2)}\right)\\ &= \mathrm{Cov}_t\left(\beta_1\sqrt{Z_t^{(0)}}dB_t+\sqrt{Z_t^{(1)}}dB_t^{(1)},\beta_2\sqrt{Z_t^{(0)}}dB_t+\sqrt{Z_t^{(1)}}dB_t^{(2)}\right)\\ &= \mathrm{Cov}_t\left(\beta_1\sqrt{Z_t^{(0)}}dB_t,\beta_2\sqrt{Z_t^{(0)}}dB_t\right)\\ &= \beta_1\beta_2 Z_t^{(0)}dt.\end{aligned}$$

Finally, we have the following correlation coefficient between the underlying asset and the counterpart's assets,

$$\mathrm{Corr}_t\left(\frac{dS}{S},\frac{dV}{V}\right) = \frac{\beta_1\beta_2 Z_t^{(0)}}{\sqrt{\beta_1^2 Z_t^{(0)}+Z_t^{(1)}}\sqrt{\beta_2^2 Z_t^{(0)}+Z_t^{(2)}}}.$$

It can be observed that the correlation coefficient between the underlying asset and the counterpart's assets changes stochastically over time, and its time-t value depends on the values of $Z_t^{(0)}$, $Z_t^{(1)}$ and $Z_t^{(2)}$.

2.3 The Approximate Pricing Formula of Vulnerable Options

In this section, we turn to the pricing formula of vulnerable European options. Since there is no closed form available in the proposed Garch Diffusion models in Subsection 2.1, here we choose to derive the approximate pricing formula by approximating the joint characteristic functions. Before doing this, we first see its exact expectation form.

As mentioned, we examine counterparty default risk using structural approaches. In line with Klein (1996) and Wang et al. (2017), we have the value of vulnerable European call options with strike price K as follows,

$$C^* = e^{-rT}E\Big[(S_T-K)^+\Big(\mathbf{1}(V_T \geq D) + \frac{(1-\alpha)V_T}{D}\mathbf{1}(V_T < D)\Big)\Big], \tag{2.4}$$

where α is the bankruptcy cost, D is a certain amount, and default occurs when the market value of the counterparty's assets V_T is less than it.

From Proposition 2.4 in Wang (2018), we could use standard probability theory and obtain the closed form of C^* in (2.4) if we have the explicit expression of the joint characteristic function of $\ln S_T$ and $\ln V_T$ defined below,

$$f(t,T;\psi_1,\psi_2) := E_t[e^{i\psi_1 \ln S_T + i\psi_2 \ln V_T}],$$

where ψ_1 and ψ_2 are real numbers.

However, in the proposed Garch Diffusion models, the explicit expression of the joint characteristic function is not available, because the proposed Garch Diffusion models belong to non-affine models. In order to complete the valuation of vulnerable options in the proposed Garch Diffusion models, here we choose to approximate the joint characteristic functions. The main idea is to employ the perturbation method to deal with the partial differential equation (PDE) for the characteristic function and obtain an approximate expression. Detailed calculations in the appendix provide us with the following approximate one,

$$\begin{aligned} f(t,T;\psi_1,\psi_2) &\approx \hat{f}(t,T;\psi_1,\psi_2) \\ &= e^{i\psi_1 \ln S_t + i\psi_2 \ln V_t + D(T-t,\psi_1,\psi_2)Z_t^{(0)} + E(T-t,\psi_1,\psi_2)Z_t^{(1)} + F(T-t,\psi_1,\psi_2)Z_t^{(2)} + G(T-t,\psi_1,\psi_2)}, \end{aligned}$$

where $D(\cdot,\cdot,\cdot)$, $E(\cdot,\cdot,\cdot)$, $F(\cdot,\cdot,\cdot)$ and $G(\cdot,\cdot,\cdot)$ are given in (A.10)-(A.13), respectively.

With the above approximate joint characteristic function in hand, we use Proposition 2.4 in Wang (2018) and could get the approximate pricing formula as follows,

$$C^* \approx e^{-r(T-t)}\Big[\Pi_1(T) - K\Pi_2(T) + \frac{1-\alpha}{D}\Big(\Pi_3(T) - K\Pi_4(T)\Big)\Big], \tag{2.5}$$

where

$$\begin{aligned}\Pi_1(T) &= \frac{1}{4}\hat{f}(0,T;-i,0) + \frac{1}{2\pi}\int_0^\infty \mathrm{Re}\Big[\frac{e^{-i\phi_1 \ln K}\hat{f}(0,T;\phi_1 - i,0)}{i\phi_1}\Big]\mathrm{d}\phi_1 \\ &\quad + \frac{1}{2\pi}\int_0^\infty \mathrm{Re}\Big[\frac{e^{-i\phi_2 \ln D}\hat{f}(0,T;-i,\phi_2)}{i\phi_2}\Big]\mathrm{d}\phi_2 \\ &\quad - \frac{1}{2\pi^2}\int_0^\infty\int_0^\infty \Big(\mathrm{Re}\Big[\frac{e^{-i\phi_1 \ln K - i\phi_2 \ln D}\hat{f}(0,T;\phi_1 - i,\phi_2)}{\phi_1\phi_2}\Big] \\ &\qquad\qquad - \mathrm{Re}\Big[\frac{e^{-i\phi_1 \ln K + i\phi_2 \ln D}\hat{f}(0,T;\phi_1 - i,-\phi_2)}{\phi_1\phi_2}\Big]\Big)\mathrm{d}\phi_1\mathrm{d}\phi_2, \end{aligned} \tag{2.6}$$

$$\begin{aligned}\Pi_2(T) &= \frac{1}{4} + \frac{1}{2\pi}\int_0^\infty \mathrm{Re}\Big[\frac{e^{-i\phi_1 \ln K}\hat{f}(0,T;\phi_1,0)}{i\phi_1}\Big]\mathrm{d}\phi_1 \\ &\quad + \frac{1}{2\pi}\int_0^\infty \mathrm{Re}\Big[\frac{e^{-i\phi_2 \ln D}\hat{f}(0,T;0,\phi_2)}{i\phi_2}\Big]\mathrm{d}\phi_2 \\ &\quad - \frac{1}{2\pi^2}\int_0^\infty\int_0^\infty \Big(\mathrm{Re}\Big[\frac{e^{-i\phi_1 \ln K - i\phi_2 \ln D}\hat{f}(0,T;\phi_1,\phi_2)}{\phi_1\phi_2}\Big] \\ &\qquad\qquad - \mathrm{Re}\Big[\frac{e^{-i\phi_1 \ln K + i\phi_2 \ln D}\hat{f}(0,T;\phi_1,-\phi_2)}{\phi_1\phi_2}\Big]\Big)\mathrm{d}\phi_1\mathrm{d}\phi_2, \end{aligned} \tag{2.7}$$

$$\begin{aligned}\Pi_3(T) &= \frac{1}{4}\hat{f}(0,T;-i,-i) + \frac{1}{2\pi}\int_0^\infty \mathrm{Re}\Big[\frac{e^{-i\phi_1 \ln K}\hat{f}(0,T;\phi_1 - i,-i)}{i\phi_1}\Big]\mathrm{d}\phi_1 \\ &\quad + \frac{1}{2\pi}\int_0^\infty \mathrm{Re}\Big[\frac{e^{-i\phi_2 \ln D}\hat{f}(0,T;-i,\phi_2 - i)}{i\phi_2}\Big]\mathrm{d}\phi_2 \\ &\quad - \frac{1}{2\pi^2}\int_0^\infty\int_0^\infty \Big(\mathrm{Re}\Big[\frac{e^{-i\phi_1 \ln K - i\phi_2 \ln D}\hat{f}(0,T;\phi_1 - i,\phi_2 - i)}{\phi_1\phi_2}\Big] \\ &\qquad\qquad - \mathrm{Re}\Big[\frac{e^{-i\phi_1 \ln K + i\phi_2 \ln D}\hat{f}(0,T;\phi_1 - i,-\phi_2 - i)}{\phi_1\phi_2}\Big]\Big)\mathrm{d}\phi_1\mathrm{d}\phi_2, \end{aligned} \tag{2.8}$$

and

$$\begin{aligned}\Pi_4(T) &= \frac{1}{4}\hat{f}(0,T;0,-i) + \frac{1}{2\pi}\int_0^\infty \mathrm{Re}\Big[\frac{e^{-i\phi_1 \ln K}\hat{f}(0,T;\phi_1,-i)}{i\phi_1}\Big]\mathrm{d}\phi_1 \\ &\quad + \frac{1}{2\pi}\int_0^\infty \mathrm{Re}\Big[\frac{e^{-i\phi_2 \ln D}\hat{f}(0,T;0,\phi_2 - i)}{i\phi_2}\Big]\mathrm{d}\phi_2 \end{aligned}$$

$$-\frac{1}{2\pi^2}\int_0^\infty\int_0^\infty\Big(\mathrm{Re}\Big[\frac{e^{-i\phi_1\ln K-i\phi_2\ln D}\hat{f}(0,T;\phi_1,\phi_2-i)}{\phi_1\phi_2}\Big] -\mathrm{Re}\Big[\frac{e^{-i\phi_1\ln K+i\phi_2\ln D}\hat{f}(0,T;\phi_1,-\phi_2-i)}{\phi_1\phi_2}\Big]\Big)\mathrm{d}\phi_1\mathrm{d}\phi_2. \quad (2.9)$$

Note that $\Pi_1(T)$-$\Pi_4(T)$ have similar forms, because they are all obtained by inverting the joint characteristic function to get the corresponding distribution function. In addition, measure change methods have been used to simplify the calculations (see, e.g., Heston (1993) and Wang (2020)).

3 Numerical Analysis

In this section, we present the pricing of European options with counterparty risk. Since they have impacts on both the issuer's assets and the underlying asset, we primarily address the implications of stochastic volatilities and systematic risk here. Additionally, by maintaining the total risk constant, we illustrate the variations in European option pricing when the underlying asset or the issuer's asset has different proportion of systematic risk. Furthermore, we display the values of European options with varying deadweight cost ratios under constant volatility models and stochastic volatility models.

Table 1: Parameter Definitions and Values

Parameter	Value	Parameter	Value
Initial price	$S(0)=10$	Initial price	$V(0)=30$
Default barrier	$D=30$	Strike price	$K=10$
Deadweight cost ratio	$\alpha=0.4$	Risk-free rate	$r=0.05$
Initial time	$t=0$	Maturity	$T=1$
Mean-reverting rate of volatility	$\kappa_0=1.15$	Long-term variance	$\theta_0=0.035$
Correlation coefficient	$\rho_0=-0.64$	Volatility of volatility	$\sigma_0=0.39$
Mean-reverting rate of volatility	$\kappa_i=2$	Long-term variance	$\theta_i=0.02$
Initial volatility value	$Z_0^{(0)}=0.02$	Initial volatility value	$Z_0^{(i)}=0.0401$
Volatility of volatility	$\sigma_i=0.7$	Correlation coefficient	$\rho_i=-0.5$
Market beta	$\beta_1=0.8$	Market beta	$\beta_2=0.8$

To determine the price of derivatives, we use the parameter values listed in Table 1 as a reference, based on previous studies. Chen (2010) reports that bonds have an average recovery rate of 0.60

across nine different aggregate states. We simplify by setting the deadweight costs α at 0.4 and D at 30. The option's maturity is assumed to be $T = 1$ year. For market index parameters, we adopt the reversion rate $\kappa_0 = 1.15$, long-term variance mean $\theta_0 = 0.035$, variance volatility $\sigma_0 = 0.39$, and correlation coefficient $\rho_0 = -0.64$, consistent with the findings of Bakshi, Cao, and Chen (1997) and Wang (2019). We set the initial variance $Z_0^{(0)}$ at 0.02 and the interest rate at 0.04. We set the market beta β_i $(i = 1, 2)$ at 0.80 and the initial idiosyncratic variance $Z_0^{(i)}$ at 0.0401 for the underlying asset and issuer's assets, leading to a total volatility of $\sqrt{\beta_i^2 Z_0^{(0)} + Z_0^{(i)}} = 0.23$ $(i = 1, 2)$. This aligns with Zhang, Zhou, and Zhu (2009), who reported that BB-rated firms have an average volatility of 0.23.

3.1 The Approximate Difference

In this subsection, we used a Monte Carlo simulation to simulate the price of vulnerable European options under Garch Diffusion Models, and we contrasted the outcome with the closed-form solutions derived from characteristic functions. Table 1 contains the parameters used in our simulations, and Table 2 summarizes the numerical findings.

Firstly, we focus on the convergence analysis of the derived pricing formulae, which involve infinite series and integrals. Specifically, we analyze the impact of the number of terms in the infinite series and the upper limit for the infinite integrals. The calculations are performed in MATLAB on a personal computer with an Intel Core i5 2.42 GHz processor, where all integrals are evaluated using the `integral` function. The results demonstrate that option prices remain stable when the upper limit of the infinite integral is set to 10^2, confirming the accuracy of the numerical integration with this setting.

Table 2: Prices of vulnerable European options with alternative maturities and strike prices under the function and the MC simulation. UL is the upper limit for the infinite integrals.

T	K	UL	Option Price	CPU	Monte Carlo	Std. Error	Difference
1	8	10^1	2.1241	2.7651	2.1087	0.001912	0.001473

Table 2: (continued)

T	K	UL	Option Price	CPU	Monte Carlo	Std. Error	Difference
		10^2	2.1055	2.8008			
		10^3	2.1055	4.5116			
		10^4	2.1055	5.6578			
	9	10^1	1.4809	2.0664	1.4784	0.001684	0.001731
		10^2	1.4759	2.1256			
		10^3	1.4759	3.3046			
		10^4	1.4759	4.7236			
	10	10^1	0.9391	2.0891	0.9583	0.001409	0.000310
		10^2	0.9580	2.1475			
		10^3	0.9580	2.7690			
		10^4	0.9580	4.7408			
	11	10^1	0.5442	2.0664	0.5724	0.001111	-0.001881
		10^2	0.5734	2.1205			
		10^3	0.5734	2.8072			
		10^4	0.5734	5.0451			
	12	10^1	0.2968	2.0364	0.3152	0.000830	-0.004679
		10^2	0.3167	2.0919			
		10^3	0.3167	2.9352			
		10^4	0.3167	4.9802			
2	8	10^1	2.5581	2.0748	2.5513	0.002638	-0.002460
		10^2	2.5576	2.1169			
		10^3	2.5576	4.6448			
		10^4	2.5576	5.0624			
	9	10^1	1.9810	2.6255	1.9732	0.002408	-0.002420
		10^2	1.9780	2.4900			
		10^3	1.9780	4.3732			

Table 2: (continued)

T	K	UL	Option Price	CPU	Monte Carlo	Std. Error	Difference
		10^4	1.9780	5.3501			
	10	10^1	1.4799	2.0565	1.4787	0.002152	-0.000464
		10^2	1.4794	2.0872			
		10^3	1.4794	3.7722			
		10^4	1.4794	4.6160			
	11	10^1	1.0675	2.0898	1.0694	0.001876	-0.001443
		10^2	1.0710	2.1095			
		10^3	1.0710	2.7708			
		10^4	1.0710	4.3335			
	12	10^1	0.7463	2.0270	0.7475	0.001594	-0.005779
		10^2	0.7519	2.1115			
		10^3	0.7519	3.4268			
		10^4	0.7519	4.7882			

For the Monte Carlo simulation, our analysis is based on the following setup: $MM = 1000,000$ simulations, with time to maturity values $T = 1$ and $T = 2$, and strike prices ranging from 8 to 12. The basic parameters include a time step $dt = 0.001$ and a risk-free rate $r = 0.05$, with the number of time steps calculated as $N = T/dt$. The results from these simulations are compared with the closed-form solutions derived using characteristic functions for vulnerable European call options.

Table 2 summarizes the simulated prices, standard errors, and analytical solutions for vulnerable European call options, including percentage differences. The results demonstrate that the Monte Carlo method is accurate, with absolute percentage differences generally less than 0.4%, indicating the reliability of our simulations. However, it requires approximately 170 seconds to produce each option price for the vulnerable European call option to ensure a small standard error. In contrast, the characteristic function method calculated option prices in about 6 seconds, showing a notable boost in efficiency. Also, the absolute percentage differences between the two methods generally remained within 0.6%, indicating the reliability of the analytical solutions.

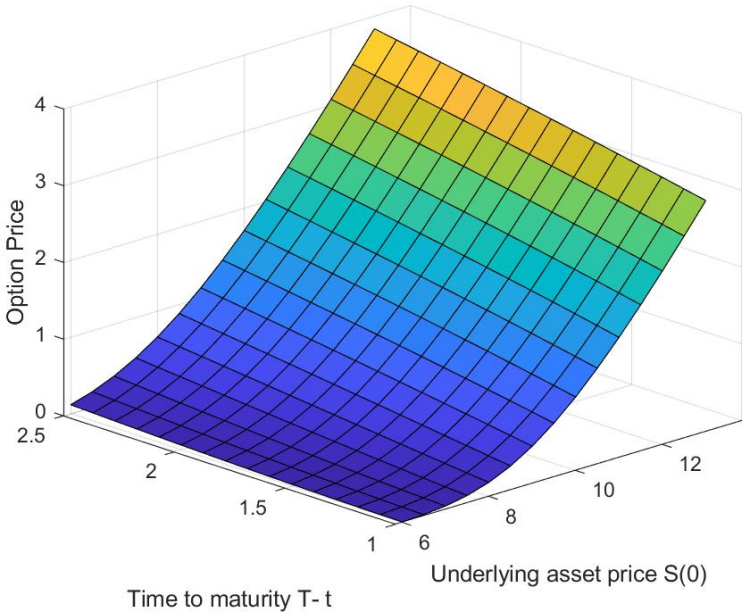

Figure 1: The option price for different S(0) and T-t

3.2 Effects of Basic Parameters

In the subsequent numerical analysis, we modify various basic parameter values to demonstrate their impact on the prices (shown in Figure 1, 2, and 3), while keeping the other parameters as specified in Table 1. These parameters include the initial price of the underlying asset, time to maturity, default barrier, and the initial value of the counterparty's asset.

Figure 1 illustrates how the initial asset price $S(0)$ and time to maturity $T-t$ affect vulnerable option prices. It is evident from the figure that an increase in $S(0)$ and a longer time to maturity result in a higher price for vulnerable options. Also, a longer time to maturity increases the chances of the asset price exceeding the exercise price, raising the option's time value. Hence, the value of the vulnerable option increases with longer time to maturity. Figure 1 also reveals the complex relationship between time to expiration and option price. With a short time to expiration, the option price is less sensitive to changes in the underlying asset price. However, as the time to expiration lengthens, the sensitivity of the option price to asset price volatility markedly increases.

The effect of different default barriers D and the time to maturity $T-t$ on the price of vulnerable options is illustrated in Figure 2. A smaller default barrier corresponds to a lower default probabil-

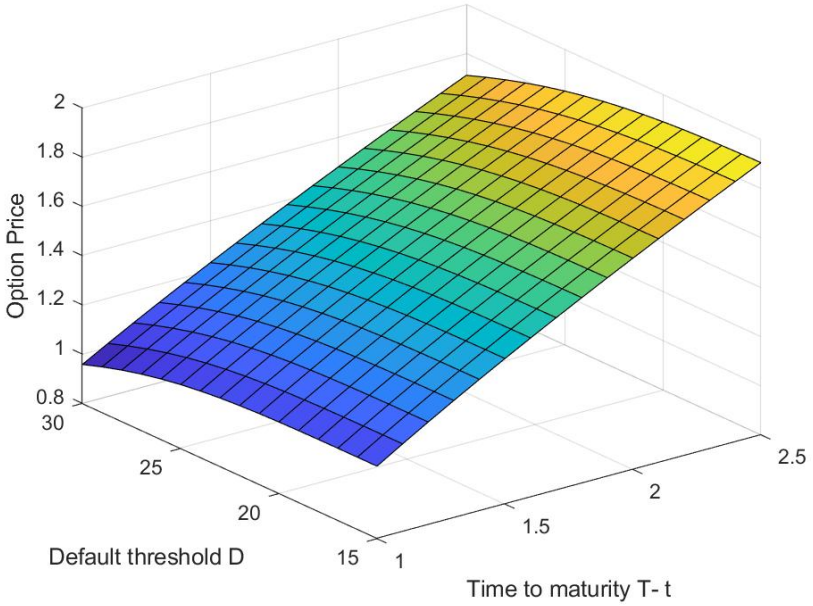

Figure 2: The option price for different D and T-t

Figure 3: The option price for different S(0) and V(0)

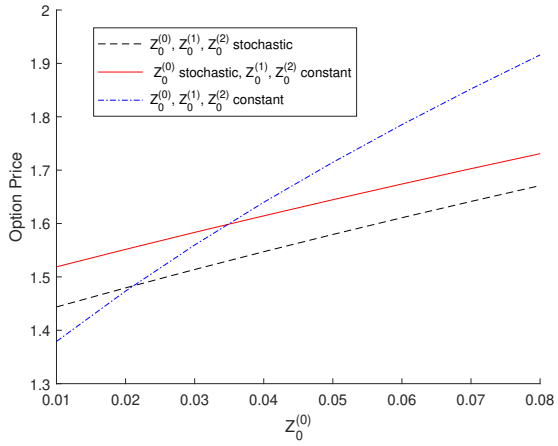

Figure 4: European call option prices against the market index's initial variance value. The proposed stochastic volatility model, the particular case of the proposed model with constant idiosyncratic volatilities of both assets, and the model in X. Wang (2017) are shown by the solid, dot-dashed, and dashed lines, respectively.

ity, implying minimal impact of counterparty credit risk on the option price. Thus, a higher default barrier D results in a lower value of the vulnerable option, which aligns with intuitive expectations.

Figure 3 displays the influence of the counterparty's asset value $V(0)$ and the underlying asset price $S(0)$ on the price of vulnerable options. The figure indicates that both a higher $S(0)$ and a higher $V(0)$ lead to an increase in the price of vulnerable options. A higher $V(0)$ raises the probability that the counterparty's asset value $V(T)$ will surpass the default threshold D at maturity, lowering the default risk. Consequently, options are more valuable when the initial counterparty's asset value $V(0)$ is higher.

3.3 Effects of Stochastic Volatilities

In this subsection, we examine the impact of stochastic volatilities. We compare the numerical results derived from our proposed model with those from X. Wang (2017), which is a specific instance of our proposed model assuming constant volatility, i.e., $Z_t^{(i)} \equiv {Z_0}^{(i)}$ $(i = 0, 1, 2)$. And We also compare the results with the constant volatilities of only the underlying asset, only the asset of the issuer, and both idiosyncratic volatilities respectively. The numerical results are shown in Figures 4-6.

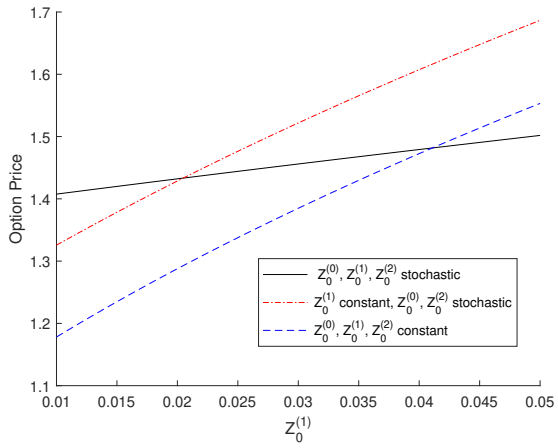

Figure 5: European call option prices against the underlying assets' initial variance value. The proposed model, the particular case of the proposed model with constant volatilities of only underlying assets,the special model with constant idiosyncratic volatilities of both assets, and the model in X. Wang (2017) are shown by the solid, dashed, dot-dashed, and dotted lines, respectively.

Firstly, the difference between option prices derived from X. Wang's (2017) model and those from the special case with constant idiosyncratic volatilities demonstrates the effect of the market index's stochastic volatility.

Figure 4 shows that European option prices with counterparty risk rise with an increase in the market index's initial variance $Z_0^{(0)}$. This result is intuitive as a higher initial variance value implies a higher initial level of total risk associated with the underlying asset. Consequently, there is a stronger initial correlation between the underlying asset and the issuer's assets, which leads to a higher option price.

On the other hand, the effect of each specific stochastic volatility can be assessed by comparing the option prices generated by the proposed model with those derived from the previously mentioned special case of the same model.

Figure 5 shows the effects of the initial idiosyncratic variance value of the underlying asset $Z_0^{(1)}$ on European call option prices. As the initial idiosyncratic variance value of the underlying asset increases, the option prices generally rise. This outcome is anticipated since a rise in $Z_0^{(1)}$ indicates a greater initial total risk for the asset, leading to higher option prices. However, a higher $Z_0^{(1)}$ also weakens the initial correlation between the underlying asset and the issuer's assets, potentially

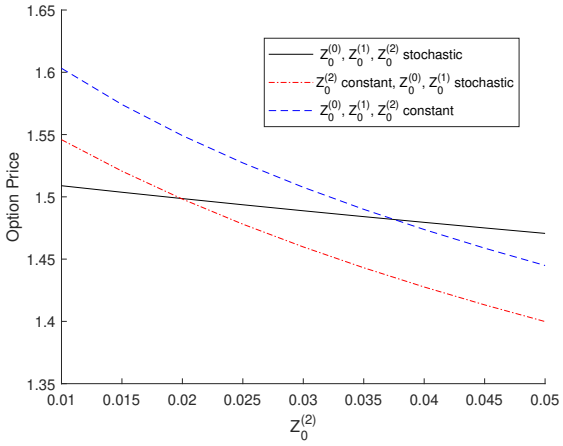

Figure 6: European call option prices against the issuers assets' initial variance value. The proposed stochastic volatility model, the particular case of the proposed model with constant idiosyncratic volatilities of only issuers assets, the special model with constant idiosyncratic volatilities of both assets, and the model in X. Wang (2017) are shown by the solid, dotted, dot-dashed, and dashed lines, respectively.

lowering option prices. The results show that as $Z_0^{(1)}$ increases, the overall option prices rise due to the total risk level of the underlying asset.

Figure 6 displays the impact of the initial idiosyncratic variance value of the issuer's assets $Z_0^{(2)}$ on European call option prices. It demonstrates that an increase in the initial variance value of the issuer's assets $Z_0^{(2)}$ generally leads to a decrease in the option prices. This is because a higher initial variance value of the counterparty's assets implies a higher default probability, which reduces the option prices. Besides, a higher $Z_0^{(2)}$ reduces the initial correlation between the underlying asset and the issuer's assets, lowering option prices. In addition, integrating stochastic volatility into the counterparty's asset ensures pricing stability, as the effect of variations in initial volatility is reduced through this incorporation.

Figures 4-6 show that using stochastic processes for counterparty asset volatility results in pricing stability, as indicated by the flatter slope of the solid line compared to constant volatility models. Considering stochastic volatility in the model makes option prices less sensitive to initial variance changes, resulting in reduced impact from market fluctuations. Therefore, incorporating stochastic volatility in pricing models leads to more accurate valuations of financial derivatives

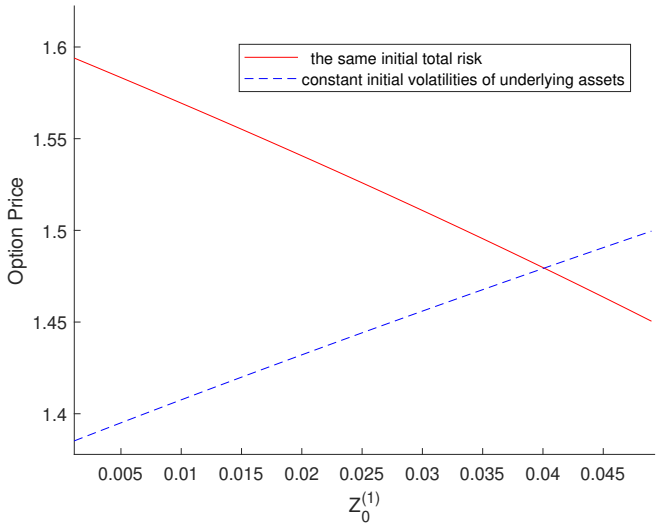

Figure 7: Impact of initial $Z_0^{(1)}$ on option prices under fixed and variable total risk

compared to constant volatility models, which can misjudge risk.

3.4 Effects of Systematic Risk

In this subsection, we analyze the effects of systematic risk by first examining the roles of $Z_0^{(1)}$ and $Z_0^{(2)}$, followed by an analysis of the market betas. Initially, we focus on how the allocation of initial idiosyncratic variances, $Z_0^{(1)}$ and $Z_0^{(2)}$, affects the total risk and, consequently, the European option prices. Specifically, we observe that redistributing $Z_0^{(1)}$ and $Z_0^{(2)}$ under a fixed total risk $\sqrt{\beta_1^2 Z_0^{(0)} + Z_0^{(i)}}$ $(i = 1, 2)$ introduces a substitution effect that alters pricing dynamics.

Figure 7 shows how the initial idiosyncratic volatility $Z_0^{(1)}$ of the underlying asset influences European call option prices in two scenarios: the red solid line indicates constant total risk through the dynamic systematic volatility $Z_0^{(0)}$, while the blue dashed line shows constant systematic volatility $Z_0^{(0)}$. The red solid line indicates higher option prices since the total risk constraint adjusts $Z_0^{(0)}$ to about 0.0827, well above the constant $Z_0^{(0)} = 0.02$ seen in the blue dashed line. However, as $Z_0^{(1)}$ increases, the red line declines because reducing $Z_0^{(0)}$ to maintain constant total risk diminishes the option's time value. This decline is further exacerbated by the higher proportion of idiosyncratic risk with long-term mean of volatility ($\theta_1 = 0.02$) compared to systematic volatility ($\theta_0 = 0.035$). Conversely, the blue dashed line shows a consistent price rise because $Z_0^{(1)}$ increases

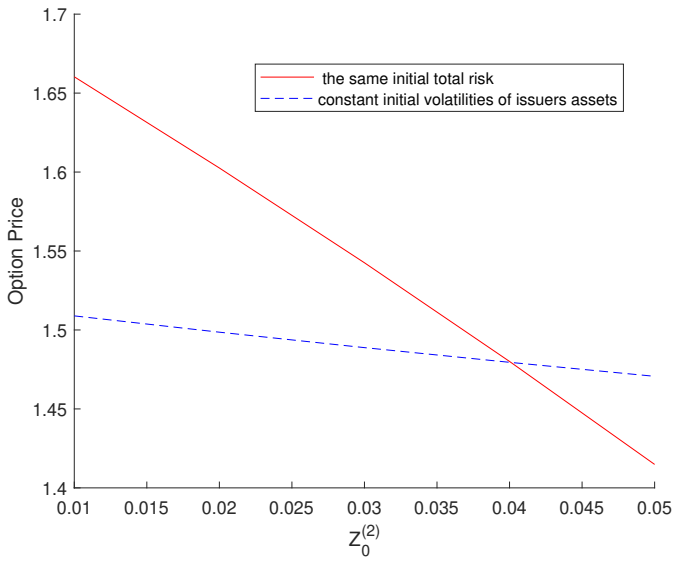

Figure 8: Impact of initial $Z_0^{(2)}$ on option prices under fixed and variable total risk. The solid line reflects the condition where total risk is fixed, balancing the distribution of $Z_0^{(1)}$ and $Z_0^{(2)}$. The dashed line represents the case where total risk increases with $Z_0^{(1)}$ while $Z_0^{(2)}$ and β remain constant.

overall volatility, raising the option's time value without decreasing $Z_0^{(0)}$. The two lines intersect at $Z_0^{(1)} = 0.0401$, where idiosyncratic risk begins to dominate in determining the total volatility. After this point, the blue dashed line exceeds the red line, indicating that $Z_0^{(1)}$ has a greater impact on total volatility and option prices while $Z_0^{(0)}$ stays fixed.

Next, we focus on the market betas (β_1 and β_2), indicating the proportions of systematic risk associated with the underlying asset and the issuer's asset. Our analysis centers on understanding how changes in systematic risk affect European call option prices. To achieve this, we examine price variations as the systematic risk of the underlying asset shifts, while keeping total risk or idiosyncratic volatilities constant. We aim to explore how systematic and idiosyncratic risks affect option pricing and the impact of market betas on vulnerable options.

Figure 9 shows how the systematic risk parameter β_1 affects option pricing in two scenarios: one with constant initial idiosyncratic volatility (blue dashed line) and the other with constant initial total risk (red solid line).

In the dashed line scenario, an increase in β_1 causes the proportion of systematic risk to gradu-

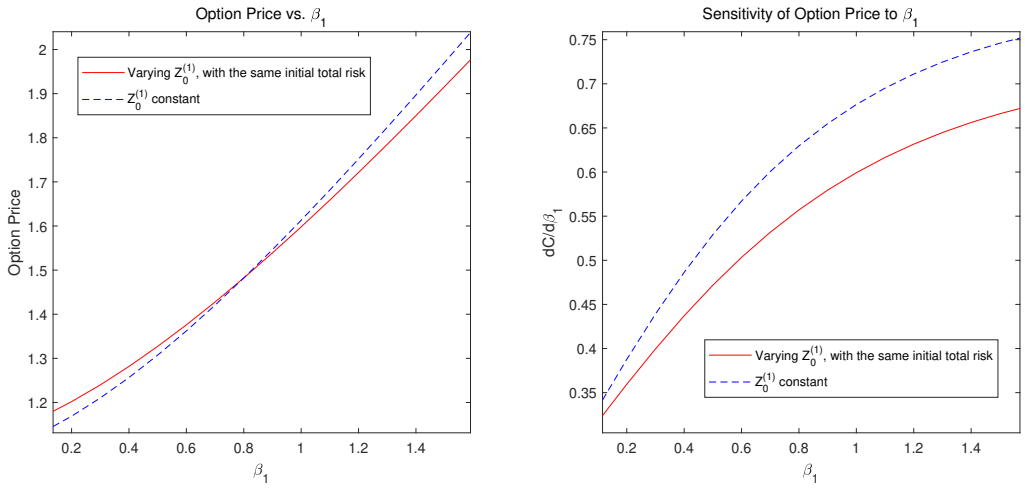

Figure 9: European call option prices against the underlying assets beta.

ally rise. Since $Z_0^{(1)}$ remains constant, total risk increases monotonically with β_1. Here, systematic risk primarily drives option pricing, leading to a steady price increase. In the early stages, when systematic risk has a smaller share, the price rises gradually. As β_1 increases, the rise in systematic risk speeds up price growth.systematic risk accelerates the price increase. While in the risk controlled scenario, the total risk $\sqrt{\beta_1^2 Z_0^{(0)} + Z_0^{(1)}}$ is kept constant. To maintain this equilibrium, $Z_0^{(1)}$ must decrease as β_1 increases. When $Z_0^{(1)}$ is high, idiosyncratic risk greatly impacts the option price, resulting in the red line being above the blue dashed line. However, beyond a critical point ($\beta_1 = 0.8$), systematic risk becomes dominant, and the reduction in $Z_0^{(1)}$ negatively impacts the price. Although the price continues to grow, the rate of increase slows compare4 d to the blue dashed line.

The sensitivity analysis (right panel) again shows these trends. The red line shows a slower increase in sensitivity as β_1 grows, reflecting the declining contribution of idiosyncratic risk in the constant total risk scenario. In contrast, the blue dashed line sensitivity rises steadily, driven by the monotonic growth of total risk.

Figure 10 presents the impact of the market beta of the issuer's asset β_2 on the European call option price under two scenarios: constant total risk (solid red line) and constant initial heterogeneous volatility (dashed blue line). Interestingly, the price curve exhibits an inverted U-shape, with the option price first increasing and then decreasing as β_2 rises. The decline of the solid red

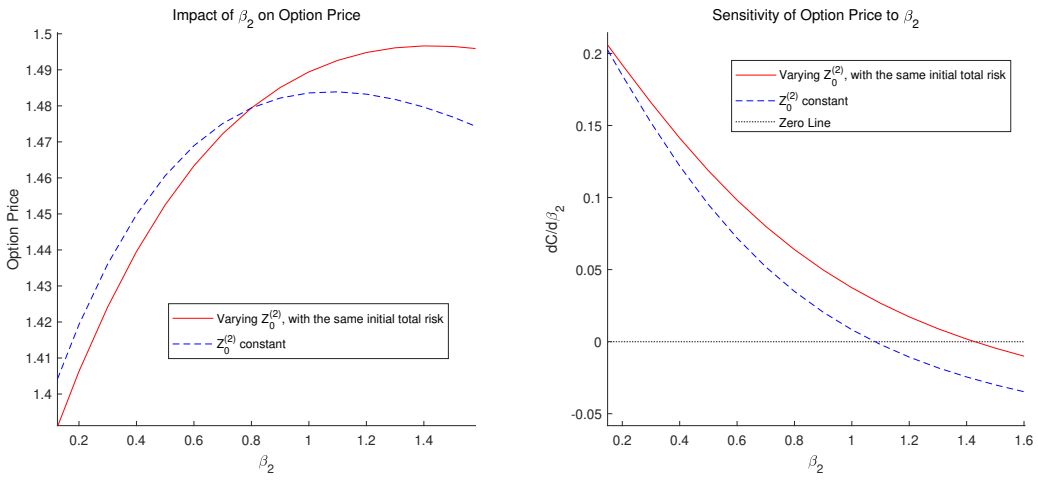

Figure 10: European call option prices and sensitivity against the issuers' assets beta

line is more gradual than that of the dashed blue line, which reflects the dynamic adjustment role of heterogeneous risk under a constant total risk scenario.

A higher β_2 indicates a stronger correlation with the market, leading to an increase in systematic volatility. Higher systematic volatility, associated with a larger long-run mean ($\theta_0 = 0.035$), reduces the probability of default and increases the option value. Moreover, an increase in aggregate volatility lifts the time value of the option, which drives up the price.

Before the intersection point, the blue dashed line price is higher than the red solid line, because the increase in systematic risk in the constant initial heterogeneous risk scenario is directly reflected in the increase in total risk, and this higher total risk enhances the time value of the option. After the intersection point, the solid red line exceeds the dashed blue line, which reflects that under the scenario of constant total risk, controlling the increase of systemic risk by dynamically reducing heterogeneous risk helps alleviate the negative impact of rising default probability on option prices.

As β_2 increases further, the option price begins to decrease. At this stage, systemic risk dominates the aggregate volatility, but its marginal contribution gradually decreases, while the negative effect of heterogeneous risk on the probability of default becomes more significant. This effect is particularly pronounced in the high β_2 region, leading to lower prices.

The right panel shows the first derivative of the option price with respect to β_2. In both scenarios, the derivative curve decreases monotonically as β_2 increases, reflecting the gradual weakening of the marginal effect of β_2 on price. The economic significance of this monotonic decrease is that

the marginal contribution of systematic risk to total risk diminishes as β_2 increases, while the negative effect of default probability at higher β_2 gradually dominates. The solid red line is always above the dashed blue line, indicating that in the constant total risk scenario, dynamic adjustment of heterogeneous risks can more effectively alleviate the negative impact of rising systemic risks. These effects eventually lead to a downward trend in the high β_2 region of the price curve and a consistently positive but diminishing marginal effect of price changes.

4 Conclusion

In this paper, we study the pricing of vulnerable options under stochastic volatility using a continuous-time Garch Diffusion model. Our analysis reveals the impact of market volatility and counterparty asset volatility on option pricing, demonstrating how the model's parameters influence the sensitivity of option values. The findings contribute to a more accurate valuation of financial derivatives in the presence of default risk and provide a foundation for further research in option pricing under stochastic volatility.

Appendix

Here we derive an approximate expression of the joint characteristic function of $\ln S_T$ and $\ln V_T$. To this end, we write it in a more clear form,

$$f\left(x,y,z,z_1,z_2,\tau;\phi_1,\phi_2\right)=E\left[e^{i\phi_1\ln S_T+i\phi_2\ln V_T}\middle|\ \ln S_t=x,\ln V_t=y,Z_t^{(0)}=z,Z_t^{(1)}=z_1,Z_t^{(2)}=z_2\right],$$

where $\tau=T-t$.

Recall that the volatility dynamics are as follows,

$$\begin{cases}\mathrm{d}Z_t^{(0)}=\kappa_0(\theta_0-Z_t^{(0)})\mathrm{d}t+\sigma_0 Z_t^{(0)}\mathrm{d}L_t,\\ \mathrm{d}Z_t^{(1)}=\kappa_1(\theta_1-Z_t^{(1)})\mathrm{d}t+\sigma_1 Z_t^{(1)}\mathrm{d}L_t^{(1)},\\ \mathrm{d}Z_t^{(2)}=\kappa_2(\theta_2-Z_t^{(2)})\mathrm{d}t+\sigma_2 Z_t^{(2)}\mathrm{d}L_t^{(2)},\end{cases}\tag{A.1}$$

and we can write $\ln S_t$ and $\ln V_t$ in the following form,

$$\begin{aligned}\mathrm{d}\ln S_t&=\left(r-\tfrac{1}{2}\beta_1^2Z_t^{(0)}-\tfrac{1}{2}Z_t^{(1)}\right)\mathrm{d}t+\beta_1\sqrt{Z_t^{(0)}}\left(\rho_0\mathrm{d}L_t+\sqrt{1-\rho_0^2}\mathrm{d}\widetilde{B}_t\right)+\sqrt{Z_t^{(1)}}\left(\rho_1\mathrm{d}L_t^{(1)}+\sqrt{1-\rho_1^2}\mathrm{d}\widetilde{B}_t^{(1)}\right),\\ \mathrm{d}\ln V_t&=\left(r-\tfrac{1}{2}\beta_2^2Z_t^{(0)}-\tfrac{1}{2}Z_t^{(2)}\right)\mathrm{d}t+\beta_2\sqrt{Z_t^{(0)}}\left(\rho_0\mathrm{d}L_t+\sqrt{1-\rho_0^2}\mathrm{d}\widetilde{B}_t\right)+\sqrt{Z_t^{(2)}}\left(\rho_2\mathrm{d}L_t^{(2)}+\sqrt{1-\rho_2^2}\mathrm{d}\widetilde{B}_t^{(2)}\right),\end{aligned}$$

where L_t, $L_t^{(1)}$, $L_t^{(2)}$, $\widetilde{B}_t$, $\widetilde{B}_t^{(1)}$ and $\widetilde{B}_t^{(2)}$ are independent standard Brownian motions.

Utilizing the Feynman-Kac theorem, we get that the characteristic function satisfies the following partial differential equation (PDE),

$$\begin{aligned}
&-\frac{\partial f}{\partial \tau}+\left(r-\tfrac{1}{2}\beta_1^2 z-\tfrac{1}{2}z_1\right)\frac{\partial f}{\partial x}+\left(\tfrac{1}{2}\beta_1^2 z+\tfrac{1}{2}z_1\right)\frac{\partial^2 f}{\partial x^2}+\left(r-\tfrac{1}{2}\beta_2^2 z-\tfrac{1}{2}z_2\right)\frac{\partial f}{\partial y}+\left(\tfrac{1}{2}\beta_2^2 z+\tfrac{1}{2}z_2\right)\frac{\partial^2 f}{\partial y^2}\\
&+\kappa_0\left(\theta_0-z\right)\frac{\partial f}{\partial z}+\tfrac{1}{2}\sigma_0^2 z^2\frac{\partial^2 f}{\partial z^2}+\kappa_1\left(\theta_1-z_1\right)\frac{\partial f}{\partial z_1}+\tfrac{1}{2}\sigma_1^2 z_1^2\frac{\partial^2 f}{\partial z_1^2}+\kappa_2\left(\theta_2-z_2\right)\frac{\partial f}{\partial z_2}+\tfrac{1}{2}\sigma_2^2 z_2^2\frac{\partial f}{\partial z_2^2}\\
&+\beta_1\beta_2 z\frac{\partial^2 f}{\partial x\partial y}+\beta_1\rho_0\sigma_0 z^{\frac{3}{2}}\frac{\partial^2 f}{\partial x\partial z}+\rho_1\sigma_1 z_1^{\frac{3}{2}}\frac{\partial^2 f}{\partial x\partial z_1}+\beta_2\rho_0\sigma_0 z^{\frac{3}{2}}\frac{\partial^2 f}{\partial y\partial z}+\rho_2\sigma_2 z_2^{\frac{3}{2}}\frac{\partial^2 f}{\partial y\partial z_2}=0, \qquad \text{(A.2)}
\end{aligned}$$

and the boundary condition is given by

$$f\left(x,y,z,z_1,z_2,0;\phi_1,\phi_2\right)=e^{i\phi_1\ln S_T+i\phi_2\ln V_T}.$$

Notably, Eq.(A.2) represents a non-linear PDE, diverging from the typical affine process solutions, thus lacking an exact analytical solution.

To navigate this complexity, we employ a perturbation method(Kevorkian et al. 1982; Chacko and Viceira 2003), approximating variables z^2, $z^{\frac{3}{2}}$, and z^2 via Taylor expansions around the variance's long-run mean. Then, we obtain

$$\begin{cases} z^2=2\theta_0 z-\theta_0^2 \\ z^{\frac{3}{2}}=\frac{3}{2}\theta_0^{\frac{1}{2}}z-\frac{1}{2}\theta_0^{\frac{3}{2}} \end{cases} \quad \begin{cases} z_1^2=2\theta z_1-\theta_1^2 \\ z_1^{\frac{3}{2}}=\frac{3}{2}\theta_1^{\frac{1}{2}}z_1-\frac{1}{2}\theta_1^{\frac{3}{2}} \end{cases} \quad \begin{cases} z_2^2=2\theta_2 z_2-\theta_2^2 \\ z_2^{\frac{3}{2}}=\frac{3}{2}\theta_2^{\frac{1}{2}}z_2-\frac{1}{2}\theta_2^{\frac{3}{2}} \end{cases}$$

This approximation yields a set of ordinary differential equations (ODEs), further analyzed under the boundary condition Eq.(A.4).

$$\begin{aligned}
&-\frac{\partial f}{\partial \tau}+\left(r-\frac{1}{2}\beta_1^2 z-\frac{1}{2}z_1\right)\frac{\partial f}{\partial x}+\left(\frac{1}{2}\beta_1^2 z+\frac{1}{2}z_1\right)\frac{\partial^2 f}{\partial x^2}+\left(r-\frac{1}{2}\beta_2^2 z-\frac{1}{2}z_2\right)\frac{\partial f}{\partial y}+\left(\frac{1}{2}\beta_2^2 z+\frac{1}{2}z_2\right)\frac{\partial^2 f}{\partial y^2}\\
&+\kappa_0\left(\theta_0-z\right)\frac{\partial f}{\partial z}+\frac{1}{2}\sigma_0^2\left(2\theta_0 z-\theta_0^2\right)\frac{\partial^2 f}{\partial z^2}+\kappa_1\left(\theta_1-z_1\right)\frac{\partial f}{\partial z_1}+\frac{1}{2}\sigma_1^2\left(2\theta_1 z_1-\theta_1^2\right)\frac{\partial^2 f}{\partial z_1^2}\\
&+\kappa_2\left(\theta_2-z_2\right)\frac{\partial f}{\partial z_2}+\frac{1}{2}\sigma_2^2\left(2\theta_2 z_2-\theta_2^2\right)\frac{\partial f}{\partial z_2^2}+\frac{\partial^2 f}{\partial x\partial z}\beta_1\rho_0\sigma_0\left(\frac{3}{2}\theta_0^{\frac{1}{2}}z-\frac{1}{2}\theta_0^{\frac{3}{2}}\right)+\frac{\partial f}{\partial x\partial z_1}\rho_1\sigma_1\left(\frac{3}{2}\theta_1^{\frac{1}{2}}z_1-\frac{1}{2}\theta_1^{\frac{3}{2}}\right) \qquad \text{(A.3)}\\
&+\frac{\partial^2 f}{\partial y\partial z}\beta_2\rho_0\sigma_0\left(\frac{3}{2}\theta_0^{\frac{1}{2}}z-\frac{1}{2}\theta_0^{\frac{3}{2}}\right)+\frac{\partial f}{\partial y\partial z_2}\rho_2\sigma_2\left(\frac{3}{2}\theta_2^{\frac{1}{2}}z_2-\frac{1}{2}\theta_2^{\frac{3}{2}}\right)+\frac{\partial f}{\partial x\partial y}\beta_1\beta_2 z=0
\end{aligned}$$

The PDE has an exponential-affine solution of the form

$f\left(x,y,z,z_1,z_2,\tau,i\phi_1,i\phi_2\right)=e^{i\phi_1 x+i\phi_2 y+D(\tau,\phi_1,\phi_2)z+E(\tau,\phi_1,\phi_2)z_1+F(\tau,\phi_1,\phi_2)z_2+G(\tau,\phi_1,\phi_2)}$,

with boundary conditions

$$D\left(0,\phi_1,\phi_2\right)=E\left(0,\phi_1,\phi_2\right)=F\left(0,\phi_1,\phi_2\right)=0. \qquad \text{(A.4)}$$

Substituting terms leads to the following ODE, introducing a general solution format

$$
\begin{aligned}
&-\left(D_\tau\left(\tau,\phi_1,\phi_2\right)z+E_\tau\left(\tau,\phi_1,\phi_2\right)z_1+F_\tau\left(\tau,\phi_1,\phi_2\right)z_2+G_\tau\left(\tau,\phi_1,\phi_2\right)\right)\\
&+\left(r-\frac{1}{2}\beta_1^2z-\frac{1}{2}z_1\right)i\phi_1+\left(\frac{1}{2}\beta_1^2z+\frac{1}{2}z_1\right)\left(i\phi_1\right)^2+\left(r-\frac{1}{2}\beta_2^2z-\frac{1}{2}z_0\right)i\phi_2+\left(\frac{1}{2}\beta_2^2z+\frac{1}{2}z_2\right)\left(i\phi_2\right)^2\\
&+\kappa_0\left(\theta_0-z\right)D\left(\tau,\phi_1,\phi_2\right)+\frac{1}{2}\sigma_0^2\left(2\theta_0z-\theta_0^2\right)D^2\left(\tau,\phi_1,\phi_2\right)\\
&+\kappa_1\left(\theta_1-z_1\right)E\left(\tau,\phi_1,\phi_2\right)+\frac{1}{2}\sigma_1^2\left(2\theta_1z_1-\theta_1^2\right)E^2\left(\tau,\phi_1,\phi_2\right)\\
&+\kappa_2\left(\theta_2-z_2\right)F\left(\tau,\phi_1,\phi_2\right)+\frac{1}{2}\sigma_2^2\left(2\theta_2z_2-\theta_2^2\right)F^2\left(\tau_1\phi_1,\phi_2\right)\\
&+\beta_1\rho_0\sigma_0\left(\frac{3}{2}\theta_0^{\frac{1}{2}}z-\frac{1}{2}\theta_0^{\frac{3}{2}}\right)i\phi_1D\left(\tau,\phi_1,\phi_2\right)+\rho_1\sigma_1\left(\frac{3}{2}\theta_1^{\frac{1}{2}}z_1-\frac{1}{2}\theta_1^{\frac{3}{2}}\right)i\phi_1E\left(\tau,\phi_1,\phi_2\right)+\left(i\phi_1\right)\left(i\phi_2\right)\beta_1\beta_2z\\
&+\beta_2\rho_0\sigma_0\left(\frac{3}{2}\theta_0^{\frac{1}{2}}z-\frac{1}{2}\theta_0^{\frac{3}{2}}\right)i\phi_2D\left(\tau_1\phi_1,\phi_2\right)+\rho_2\sigma_2\left(\frac{3}{2}\theta_2^{\frac{1}{2}}z_2-\frac{1}{2}\theta_2^{\frac{3}{2}}\right)i\phi_2F\left(\tau,\phi_1,\phi_2\right)=0.
\end{aligned}
\tag{A.5}
$$

Matching coefficients of z allows us to extract the following ODE

$$
\begin{aligned}
D_\tau\left(\tau,\phi_1,\phi_2\right)=&-\frac{1}{2}\left(\left(\beta_1^2\phi_1+\beta_2^2\phi_2\right)i+\left(\beta_1\phi_1+\beta_2\phi_2\right)^2\right)\\
&+\left(\frac{3}{2}\rho_0\sigma_0\theta_0^{\frac{1}{2}}\left(\beta_1\phi_1i+\beta_2\phi_2i\right)-\kappa_0\right)D\left(\tau,\phi_1,\phi_2\right)+\sigma_0^2\theta_0D^2\left(\tau,\phi_1,\phi_2\right)
\end{aligned}
\tag{A.6}
$$

Likewise, by matching coefficients of z_1 and z_2 respectively we can derive

$$
E_\tau\left(\tau,\phi_1,\phi_2\right)=-\frac{1}{2}i\phi_1-\frac{1}{2}\phi_1^2+\left(\rho_1\sigma_1\frac{3}{2}\theta_1^{\frac{1}{2}}\phi_1i-\kappa_1\right)E\left(\tau,\phi_1,\phi_2\right)+\sigma_1^2\theta_1E^2\left(\tau,\phi_1,\phi_2\right),
\tag{A.7}
$$

and

$$
F_\tau\left(\tau,\phi_1,\phi_2\right)=-\frac{1}{2}i\phi_2-\frac{1}{2}\phi_2^2+\left(\rho_2\sigma_2\frac{3}{2}\theta_2^{\frac{1}{2}}\phi_2i-\kappa_2\right)F\left(\tau,\phi_1,\phi_2\right)+\sigma_2^2\theta_2F^2\left(\tau,\phi_1,\phi_2\right).
\tag{A.8}
$$

We then focus on (A.6) , for which a general solution applicable to the Riccati equation is identified as follows

$$
D_\tau\left(\tau,\phi_1,\phi_2\right)=d_2D^2\left(\tau,\phi_1,\phi_2\right)+d_1D\left(\tau,\phi_1,\phi_2\right)+d_0.
\tag{A.9}
$$

where $d_2=\sigma_0^2\theta_0$, $d_1=\frac{3}{2}\rho_0\sigma_0\theta_0^{\frac{1}{2}}\left(\beta_1\phi_1i+\beta_2\phi_2i\right)-\kappa_0$, $d_0=-\frac{1}{2}\left(\left(\beta_1^2\phi_1+\beta_2^2\phi_2\right)i+\left(\beta_1\phi_1+\beta_2\phi_2\right)^2\right)$

Making the subsitution $D\left(\tau,\phi_1,\phi_2\right)=-\frac{O'(\tau)}{d_2O(\tau)}$ into (A.9), we can obtain $O''(\tau)-d_1O'(\tau)+d_0d_2O(\tau)=0$.

Then, the general solution of the Riccati equation leads to

$$
D\left(\tau,\phi_1,\phi_2\right)=-\frac{1}{d_2}\frac{-\frac{O(0)\omega_{1+}\omega_{1-}}{\zeta_1}e^{\omega_{1+}\tau}+\frac{O(0)\omega_{1+}\omega_{1-}}{\zeta_1}e^{\omega_{1-}\tau}}{-\frac{O(0)\omega_{1-}}{\zeta_1}e^{\omega_{1+}\tau}+\frac{O(0)\omega_{1+}}{\zeta_1}e^{\omega_{1-}\tau}}=d_0\frac{1-e^{-\zeta_1\tau}}{-\omega_{1-}+\omega_{1+}e^{-\zeta_1\tau}},
\tag{A.10}
$$

where

$$\zeta_1 = \sqrt{d_1^2 - 4d_0d_2} \quad \omega_{1\pm} = \frac{d_1 \pm \sqrt{d_1^2 - 4d_0d_2}}{2}.$$

Through parallel deduction, we have

$$E(\tau, \phi_1, \phi_2) = e_0 \frac{1-e^{-\zeta_2\tau}}{-\omega_{2-}+\omega_{2+}e^{-\zeta_2\tau}} \quad \zeta_2 = \sqrt{e_1^2 - 4e_0e_2} \quad \omega_{2\pm} = \frac{e_1 \pm \sqrt{e_1^2-4e_0e_2}}{2}, \tag{A.11}$$

$$F(\tau, \phi_1, \phi_2) = f_0 \frac{1 - e^{-\xi_3\tau}}{-\omega_{3-} + \omega_{3+}e^{-\zeta_3\tau}} \quad \zeta_3 = \sqrt{f_1^2 - 4f_0f_1} \quad \omega_{3\pm} = \frac{f_1 \pm \sqrt{f_1^2 - 4f_0f_2}}{2}. \tag{A.12}$$

where we have

$$\begin{cases} e_0 = -\frac{1}{2}i\phi_1 - \frac{1}{2}\phi_1^2 \\ e_1 = \rho_1\sigma_1\frac{3}{2}\theta_1^{\frac{1}{2}}\phi_1 i - \kappa_1 \\ e_2 = \sigma_1^2\theta_1 \end{cases} \text{ and } \begin{cases} f_0 = -\frac{1}{2}i\phi_2 - \frac{1}{2}\phi_2^2 \\ f_1 = \rho_2\sigma_2\frac{3}{2}\theta_2^{\frac{1}{2}}\phi_2 i - \kappa_2 \\ f_2 = \sigma_2^2\theta_2. \end{cases}$$

Substituting (A.6) (A.7),(A.8) into (A.5) and matching the coefficients of constant results in

$$\begin{aligned} G\tau(\tau, \phi_1, \phi_2) &= ri\phi_1 + ri\phi_2 + \kappa_0\theta_0 D(\tau, \phi_1, \phi_2) - \frac{1}{2}\sigma_0^2\theta_0^2 D^2(\tau_1, \phi_1, \phi_2) \\ &+ \kappa_1\theta_1 E(\tau, \phi_1, \phi_2) - \frac{1}{2}\sigma_1^2\theta_1^2 E^2(\tau, \phi_1, \phi_2) + \kappa_2\theta_2 F(\tau, \phi_1, \phi_2) - \frac{1}{2}\sigma_2^2\theta_2^2 F^2(\tau, \phi_1, \phi_2) \\ &- \beta_1\rho_0\sigma_0\frac{1}{2}\theta_0^{\frac{3}{3}} i\phi_1 D(\tau, \phi_{11}\phi_2) - \frac{1}{2}\rho_1\sigma_1\theta_1^{\frac{3}{2}} i\phi_1 E(\tau, \phi_1\phi_2) \\ &- \beta_2\rho_0\sigma_0\frac{1}{2}\theta_0^{\frac{3}{2}} i\phi_2 D(\tau, \phi_1, \phi_2) - \frac{1}{2}\rho_2\sigma_2\theta_2^{\frac{3}{2}} i\phi_2 F(\tau, \phi_1, \phi_2) \\ &= ri(\phi_1 + \phi_2) + \left(-\frac{1}{2}\beta_0\sigma_0\theta_0^{\frac{3}{2}} i(\beta_1\phi_1 + \beta_2\phi_2) + \kappa_0\theta_0\right) D(\tau, \phi_1, \phi_2) - \frac{1}{2}\sigma_0^2\theta_0^2 D^2(\tau, \phi_1, \phi_2) \\ &+ \left(\kappa_1\theta_1 - \frac{1}{2}\rho_1\sigma_1\theta_1^{\frac{3}{2}} i\phi_1\right) E(\tau, \phi_1, \phi_2) - \frac{1}{2}\sigma_1^2\theta_1^2 E^2(\tau, \phi_1, \phi_2) \\ &+ \left(\kappa_2\theta_2 - \frac{1}{2}\rho_2\sigma_2\theta_2^{\frac{3}{2}} i\phi_2\right) F(\tau, \phi_1, \phi_2) - \frac{1}{2}\sigma_2^2\theta_2^2 F^2(\tau, \phi_1, \phi_2). \end{aligned}$$

Multiplying both sides of equation (A.6) by $-\frac{1}{2}\theta_0$ leads to further developments

$$\begin{aligned} -\frac{1}{2}\sigma_0^2\theta_0^2 D^2(\tau, \phi_1, \phi_2) = -\frac{1}{2}\theta_0 \Bigg[& D_\tau(\tau, \phi_1, \phi_2) + \frac{1}{2}\left(\left(\beta_1^2\phi_1 + \beta_2^2\phi_2\right) i + (\beta_1\phi_1 + \beta_2\phi_2)^2\right) \\ & - \left(\frac{3}{2}\rho_0\sigma_0\theta_0^{\frac{1}{2}}(\beta_1\phi_1 i + \beta_2\phi_2 i) - \kappa_0\right) D(\tau, \phi_1\phi_2)\Bigg]. \end{aligned}$$

Correspondingly, multiplying both sides of equation (A.7) and (A.8) by $-\frac{1}{2}\theta_1$ and $-\frac{1}{2}\theta_2$ respectively leads to

$$\begin{aligned} -\frac{1}{2}\sigma_1^2\theta_1^2 E^2(\tau, \phi_1, \phi_2) &= -\frac{1}{2}\theta_1\left[E\tau(\tau, \phi_1, \phi_2) + \frac{1}{2}i\phi_1 + \frac{1}{2}\phi_1^2 - \left(\rho_1\sigma_1\frac{3}{2}\theta_1^{\frac{3}{2}}\phi_1 i - \kappa_1\right) E(\tau, \phi_1, \phi_2)\right)\Bigg] \\ -\frac{1}{2}\sigma_2^2\theta_2^2 F^2(\tau, \phi_1, \phi_2) &= -\frac{1}{2}\theta_2\left[F\tau(\tau, \phi_1, \phi_2) + \frac{1}{2}i\phi_2 + \frac{1}{2}\phi_2^2 - \left(\rho_2\sigma_2\frac{3}{2}\theta_1^{\frac{3}{2}}\phi_2 i - \kappa_2\right) F(\tau, \phi_1, \phi_2)\right)\Bigg]. \end{aligned}$$

Substituting three equations into $G_\tau(\tau,\phi_1,\phi_2)$ provides an explicit expression for $G(\tau,\phi_1,\phi_2)$.

$$\begin{aligned}
G_\tau(\tau,\phi_1,\phi_2) =& ri(\phi_1+\phi_2) - \frac{1}{2}\theta_0 D_\tau(\tau,\phi_1,\phi_2) - \frac{1}{2}\theta_1 E_\tau(\tau,\phi_1,\phi_2) - \frac{1}{2}\theta_2 F_\tau(\tau,\phi_1,\phi_2) \\
&- \frac{1}{4}\theta_0\left(\left(\beta_1^2\phi_1+\beta_2^2\phi_2\right)i + \left(\beta_1\phi_1+\beta_2\phi_2\right)^2\right) - \frac{1}{4}\theta_1\phi_1(i+\phi_1) - \frac{1}{4}\theta_2\phi_2(i+\phi_2) \\
&+ \left(\frac{1}{4}\theta_0^{\frac{3}{2}}\rho_0\sigma_0 i(\beta_1\phi_1+\beta_2\phi_2) + \frac{1}{2}\kappa_0\theta_0\right) D(\tau,\phi_1,\phi_2) \\
&+ \left(\frac{1}{4}\theta_1^{\frac{3}{2}}\rho_1\sigma_1 i\phi_1 + \frac{1}{2}\kappa_1\theta_1\right) E(\tau,\phi_1,\phi_2) + \left(\frac{1}{4}\theta_1^{\frac{3}{2}}\rho_2\sigma_2 i\phi_2 + \frac{1}{2}\kappa_2\theta_2\right) F(\tau,\phi_1,\phi_2)
\end{aligned}$$

Integrating both sides yields,

$$\begin{aligned}
G(\tau,\phi_1,\phi_2) =& ri(\phi_1+\phi_2)\tau - \frac{1}{2}\theta_0 D(\tau,\phi_1,\phi_2) - \frac{1}{2}\theta_1 E(\tau,\phi_1,\phi_2) - \frac{1}{2}\theta_2 F(\tau,\phi_1,\phi_2) \\
&- \frac{1}{4}\left(\theta_0\left(\left(\beta_1^2\phi_1+\beta_2^2\phi_2\right)i + \left(\beta_1\phi_1+\beta_2\phi_2\right)^2\right) - \theta_1\phi_1(i+\phi_1) - \theta_2\phi_2(i+\phi_2)\right)\tau \\
&+ \int_0^\tau \left(\frac{1}{4}\theta_0^{\frac{3}{2}}\rho_0\sigma_0 i(\beta_1\phi_1+\beta_2\phi_2) + \frac{1}{2}\kappa_0\theta_0\right) D(u,\phi_1,\phi_2)\,du \\
&+ \int_0^\tau \left(\frac{1}{4}\theta_1^{\frac{3}{2}}\rho_1\phi_1 i\phi_1 + \frac{1}{2}\kappa_1\theta_1\right) E(u,\phi_1,\phi_2)\,du \\
&+ \int_0^\tau \left(\frac{1}{4}\theta_1^{\frac{3}{2}}\rho_2\sigma_2 i\phi_2 + \frac{1}{2}\kappa_2\theta_2\right) F(u,\phi_1,\phi_2)\,du.
\end{aligned}$$

$$\begin{aligned}
\int_0^\tau d_3 D(u,\phi_1,\phi_2)\,du &= -\frac{d_3}{d_2}\int_0^\tau \frac{O'(u)}{O(u)}du = -\frac{d_3}{d_2}\left(\ln O(u)|_0^\tau\right) = -\frac{d_3}{d_2}\ln\left[\frac{O(\tau)}{O(0)}\right] \\
&= -\frac{d_3}{d_2}\ln\left(\frac{\frac{-O(0)\omega_{1-}}{\zeta_1}e^{\omega_{1+}\tau} + \frac{O(0)\omega_{1+}}{\zeta_1}e^{\omega_{1-}\tau}}{\frac{-O(0)\omega_{1-}}{\zeta_1} + \frac{O(0)\omega_{1+}}{\zeta_1}}\right) \\
&= -\frac{d_3}{d_2}\left[\omega_{1+}\tau + \ln\left(\frac{-\omega_{1-}+\omega_{1+}e^{-\zeta_1\tau}}{\zeta_1}\right)\right]
\end{aligned}$$

Equivalently, this results in

$$\begin{aligned}
\int_0^\tau e_3 E(u,\phi_1,\phi_2)\,du &= -\frac{e_3}{e_2}\left[\omega_{2+}\tau + \ln\left(\frac{-\omega_{2-}+\omega_{2+}e^{-\zeta_2\tau}}{\zeta_2}\right)\right] \\
\int_0^\tau f_3 F(u,\phi_1,\phi_2)\,du &= -\frac{f_3}{f_2}\left[\omega_{3+}\tau + \ln\left(\frac{-\omega_{3-}+\omega_{3+}e^{-\zeta_3\tau}}{\zeta_3}\right)\right]
\end{aligned}$$

Ultimately, this culminates in the derived expression for $G(\tau,\phi_1,\phi_2)$

$$\begin{aligned}
G(\tau,\phi_1,\phi_2) \;=\; & ri(\phi_1+\phi_2)\tau - \frac{1}{2}\left(\theta_0 D(\tau,\phi_1,\phi_2) + \theta_1 E(\tau,\phi_1,\phi_2) + \theta_2 F(\tau,\phi_1,\phi_2)\right) \\
&- \frac{1}{4}\left[\theta_0\left(\beta_1^2\phi_1+\beta_2^2\phi_2\right)i + \left(\beta_1\phi_1+\beta_2\phi_2\right)^2\right) + \theta_1\left(\phi_1 i + \phi_1^2\right) + \theta_2\left(\phi_2 i + \phi_2^2\right)\Bigg]\tau \\
&- \frac{d_3}{d_2}\left[\omega_{1+}\tau + \ln\left(\frac{-\omega_{1-}+\omega_{1+}e^{-\zeta_1\tau}}{\zeta_1}\right)\right] - \frac{e_3}{e_2}\left[\omega_{2+}\tau + \ln\left(\frac{-\omega_{2-}+\omega_{2+}e^{-\zeta_2\tau}}{\zeta_2}\right)\right]
\end{aligned}$$

$$-\frac{f_3}{f^2}\left[\omega_{3+}\tau+\ln\left(\frac{-\omega_{3-}+\omega_{3+}e^{-\zeta_3\tau}}{\zeta_3}\right)\right], \tag{A.13}$$

where

$$d_3=\frac{1}{4}\theta_0^{\frac{3}{2}}\rho_0\sigma_0 i\left(\beta_1\phi_1+\beta_2\phi_2\right)+\frac{1}{2}\kappa_0\theta_0,\quad e_3=\frac{1}{4}\theta_1^{\frac{3}{2}}\rho_1\phi_1 i\phi_1+\frac{1}{2}\kappa_1\theta_1\quad and\quad f_3=\frac{1}{4}\theta_1^{\frac{3}{2}}\rho_2\sigma_2 i\phi_2+\frac{1}{2}\kappa_2\theta_2$$

References

[1] Arora, N., Gandhi, P., & Longstaff, F. A. (2012). Counterparty credit risk and the credit default swap market. Journal of Financial Economics, 103(2), 280-293.

[2] Bollerslev, T. (1986).I Generalized autoregressive conditional heteroskedasticity. Journal of Econometrics, 31(3), 307-327.

[3] Brigo, D., Capponi, A., & Pallavicini, A. (2014). Arbitrage-free bilateral counterparty risk valuation under collateralization and application to credit default swaps. Mathematical Finance, 24(1), 125-146.

[4] Christoffersen, P., Jacobs, K., & Mimouni, K. (2007). Models for S&P 500 dynamics: Evidence from realized volatility, daily returns, and option prices. SSRN Electronic Journal.

[5] Crepey, S. (2012). Bilateral counterparty risk under funding constraints-part i: pricing. Mathematical Finance, 25(1), 1-22. https://doi.org/10.1111/mafi.12004

[6] Crepey, S. (2012). Bilateral counterparty risk under funding constraints-part ii: cva. Mathematical Finance, 25(1), 23-50. https://doi.org/10.1111/mafi.12005

[7] Genon-Catalot, V., Jeantheau, T., & Laredo, C. (2000). Stochastic volatility models as hidden Markov models and statistical applications. Bernoulli, 1051-1079.

[8] Guo, D. (1996). The predictive power of implied stochastic variance from currency options. Journal of Futures Markets, 16(8), 915-942.

[9] Heston, S. L. (1993). A closed-form solution for options with stochastic volatility with applications to bond and currency options. Review of Financial Studies, 6(2), 327-343.

[10] Johnson, H., & Stulz, R. (1987). The pricing of options with default risk. The Journal of Finance, 42(2), 267.

[11] Klein, P. (1996). Pricing black-scholes options with correlated credit risk. Journal of Banking & Finance, 20(7), 1211-1229.

[12] Liao, S.-L., & Huang, H.-H. (2005). Pricing black-scholes options with correlated interest rate risk and credit risk: An extension. Quantitative Finance, 5(5), 443-457.

[13] Ma, C., Yue, S., Wu, H., & Ma, Y. (2020). Pricing vulnerable options with stochastic volatility and stochastic interest rate. Computational Economics, 56(2), 391-429.

[14] Nelson, D. B. (1990). Arch models as diffusion approximations. Journal of Econometrics, 45(1-2), 7-38.

[15] Wang, X. (2017), Differences in the Prices of Vulnerable Options with Different Counterparties. Journal of Futures Markets, 37: 148-163. https://doi.org/10.1002/fut.21789

[16] Wang, X. (2018). Pricing vulnerable European options with stochastic correlation. Probability in the Engineering and Informational Sciences, 32(1), 67-95.

[17] Wang, X. (2020). Analytical valuation of Asian options with counterparty risk under stochastic volatility models. Journal of Futures Markets, 40(3), 410-429.

[18] Wang, X., Song, S., & Wang, Y. (2017). The valuation of power exchange options with counterparty risk and jump risk. Journal of Futures Markets, 37(5), 499-521.

[19] Xu, X., & Taylor, S. J. (1994). The term structure of volatility implied by foreign exchange options. Journal of Financial and Quantitative Analysis, 29(1), 57-74.